Vulnerability to flash floods: a simplified structural model for masonry buildings

Luca Milanesi [a]*, Marco Pilotti [a], Andrea Belleri [b], Alessandra Marini [b] and Sven Fuchs [c]

[a]*Department of Civil, Environmental, Architectural Engineering and Mathematics University of Brescia, Brescia, Italy*

[b]*Department of Engineering and Applies Sciences, University of Bergamo, Bergamo, Italy*

[c]*Institute of Mountain Risk Engineering, University of Natural Resources and Life Sciences, Vienna, Austria*

**Corresponding author*

e-mail: luca.milanesi@unibs.it

Address: Department of Civil, Environmental, Architectural Engineering and Mathematics, University of Brescia. Via Branze, 43 - 25123 Brescia (BS) Italy

Highlights

- A conceptual model to assess buildings structural vulnerability to flash floods is provided
- The model is conceived for application on large stocks of masonry buildings
- Only geometrical data to be collected via field surveys are required
- The model was positively compared with a finite elements analysis
- An example of application to real buildings in the alpine area is provided

This article has been accepted for publication and undergone full peer review but has not been through the copyediting, typesetting, pagination and proofreading process which may lead to differences between this version and the Version of Record. Please cite this article as doi: 10.1029/2018WR022577

Abstract

Urban and land use planning is conditioned by flood risk analyses and is a great research challenge. While methods are available for quantitative hazard and risk modeling, there is still a major gap related to reliable rational approaches for vulnerability assessment. This is particularly true for assessing vulnerability of buildings to floods. This vulnerability, which is important for economic reasons as well as for the safety of individuals and communities, is usually conceptualized on an empirical basis. Such empirical approaches, however, are plagued by considerable uncertainties, mostly because the damage-causing mechanisms on the building envelope are poorly represented.

In order to advance this area, this paper focuses on the structural vulnerability of traditional masonry buildings in alpine areas exposed to flash floods. A simplified physically-based conceptual model which requires a limited amount of input data is proposed. The resistance of a wall impacted by a flash flood is studied in a limit analysis framework, considering different geometric ratios and building configurations. The resulting stability thresholds, expressed in dimensionless form as a function of the water depth, were positively compared with the results provided by numerical finite element models of the investigated geometries. The application of the proposed vulnerability model in risk mitigation strategies provides reliable information, suitable for a first-level risk assessment on large building stocks.

1. Introduction

The increasing economic and social implications of floods require growing efforts for their forecast and control, as well as for the quantification of the associated societal risk [e.g., *Molinari et al.*, 2014]. Although the definition of risk formally involves the same components (i.e., hazard, vulnerability and exposure), floods in different areas are caused by different mechanisms and, accordingly, the importance of each risk parameter and its influence on the overall risk height is different.

Focusing on floods in mountain areas, these events are among the most dangerous hazards worldwide [*Santi et al.*, 2011]. In Europe [e.g., *Guzzetti et al.*, 2005; Hilker et al., 2009; *Röthlisberger et al.*, 2017; *Fuchs et al.*, 2017], in spite of a long history of hazard mitigation [*Holub and Fuchs*, 2009; *Kienholz et al.*, 2004], the overall risk is still growing due to increasing exposure [*Fuchs et al.*, 2015] and to the potential effects of climate change on the frequency and magnitude of hazards [*Keiler et al.*, 2010]. These floods are often a consequence of destructive torrential processes originating from high-intensity rainfalls or dam breaks [e.g., *Hungr*, 2008; *Iverson*, 2004; *Jakob and Hungr*, 2005].

Advanced numerical methods have been proposed for their modeling [e.g., *Ancey et al.*, 2008; *Alcrudo and Mulet*, 2007; *Costabile et al.*, 2012; *Pilotti et al.*, 2011, 2013 and 2014; *Soares-Frazão and Zech*, 2007]. However, we observe that the interaction between the hazard process and the exposed elements (i.e., vulnerability) has so far gained much less attention, leading to shortcomings in tailored risk mitigation strategies [*Mazzorana et al.*, 2014]. Therefore, vulnerability modeling is of paramount importance and its evaluation is a key step in the chain of flood risk assessment since it links flood hazard to exposure metrics providing an estimate of the expected damage and loss. So far, vulnerability was mainly explored with studies on the assessment of direct potential damage to structures [*Armanini et al.*, 2011; *Jakob et al.*, 2012; *Mazzorana et al.*, 2014], people [e.g. *Milanesi et al.*, 2015 and 2016; *Xia et al.*, 2014], network infrastructures [e.g. *Serre et al.*, 2011] and vehicles [e.g. *Arrighi et al.*, 2015; *Martinéz-Gomariz et al.*, 2016].

The hazardous nature of floods in mountain areas often arises from their destructive interaction with the built environment and the assessment of structural vulnerability of buildings is still an emerging topic. Initially, some scholars studied the overall building stability with respect to floating and horizontal forces exerted by flow [e.g. *Black*, 1975; *Dale et al.*, 2004]. With increasing availability of computational resources and mathematical models, empirical vulnerability functions based on the comparative observations between damage in real events

and flood propagation models were also suggested [e.g. *Sangrey et al.*, 1975; *Clausen and Clark*, 1990; *Karvonen at al.*, 2000, *Pilotti et al.*, 2016]. *Fuchs et al.* [2007] proposed an empirically-based preliminary vulnerability function for buildings exposed to torrential hazards in Austria. Using the same approach for a debris flow event in the Italian Alps, *Akbas et al.* [2009] showed a higher degree of loss than reported in the Austrian study. Based on a torrent event in the Italian Alps, *Papathoma-Köhle et al.* [2012] highlighted the uncertainty in the computation of empirical vulnerability curves related to the overall lack of data.

In general, these studies on the vulnerability of buildings exposed to flooding have been based on a limited knowledge of the structural characteristics of the impacted buildings so that, as suggested by *Papathoma-Köhle et al.* [2017], there is a need for more physically-based approaches. In this direction, it seems essential to understand the physical interactions between exposed buildings and the impacting processes [*Mazzorana et al.*, 2014], an issue recently addressed also in the so-called socio-hydrology debate [*Loucks*, 2015; *Di Baldassarre et al.*, 2015].

To this purpose, although field data would be necessary for model set up, calibration and validation, the available information is still scarce and in most cases the characteristics of the impacting flow are observed at monitoring stations in the catchment rather than in close proximity to the affected buildings [*Papathoma-Köhle et al.*, 2017]. Moreover, the interaction between structural elements (such as the building envelope) and the hazard depends on the flow direction, on the potential sediment concentration and size, as well as on the construction material and on the geometrical characteristics and conditions of the affected buildings [*Gems et al.*, 2016; *Papathoma-Köhle et al.*, 2017]. In order to overcome these challenges, laboratory experiments can be used to determine the process magnitude [e.g., *Cuomo et al.*, 2009], the impact on the building envelopes and the reaction of the structures to the specific impact [*Gems et al.*, 2016; *Sturm et al.*, 2018]. Experiments and modelling provide information to complement the empirical data used to date [*Armanini et al.*, 2011], yielding a unified explanation of the differing behavior of various building categories [*Totschnig and Fuchs*, 2013].

This paper contributes to this discussion, providing a physically-based structural vulnerability model for masonry buildings to flash floods caused by the sudden response of the basins to intense precipitation or dam failure [e.g., *Karagiorgos et al.*, 2016; *Alexander et al.*, 2016].

A comprehensive analysis of the stability of an individual building under flow impact requires detailed knowledge of its structural characteristics, mechanical properties of the construction materials and the state of preservation. The retrieval of these information as well as the required

computational effort are extremely challenging especially when assessing flood risk on a large building stock. On the other hand, a preliminary classification of the most exposed buildings is often needed for land planning and civil protection. Accordingly, we propose a simplified structural vulnerability model based on a set of reasonable assumptions and simple parameters to be acquired with on-site data-collection campaigns, regarding basic geometric features (main dimensions of the walls, layout of the openings, number of floors, etc.) and construction technology. Such information lead to an evaluation of the internal and external boundary conditions, of the actions transferred across adjoining elements, and of the gravitational loads. Masonry buildings are typical of traditional mountain settlements in small basins (Fig. 1) and are often characterized by stone or brick masonry structures with one or two floors. Whereas most studies consider the buildings' overall loss of stability, masonry structures have load bearing walls. Accordingly, in the collapse of a single wall might potentially destabilize the entire building so that the stability analysis must consider the behavior of each individual structural element [as done with reference to cavity walls by *Kelman and Spence*, 2003]. Accordingly, in this paper the stability of a masonry wall impacted by flow under different building configurations is addressed. The computed vulnerability thresholds, positively compared with the results of a finite elements model (FEM), are presented in dimensionless form as a function of different wall aspect ratios, in order to provide a straightforward way to identify the maximum admissible thrust on the impacted wall.

The proposed vulnerability thresholds allow for the identification of potential structural damages based on specific constructive parameters, and may therefore be of considerable value in operational risk management both from a scientific and practitioners' side. If required, buildings experiencing high potential damages may be further investigated using more detailed approaches. We believe that the resulting risk classification may be adopted by local planning authorities as a useful decision-making tool to supply, prioritize and design possible flood risk mitigation measures, including financial incentives and subsidies [*Holub and Fuchs*, 2009].

2. Methods

This study considers the effects of the impact of a flash flood on traditional masonry buildings. These structures are characterized by load bearing masonry walls whose collapse may compromise the building stability. Hence, the following vulnerability analyses will be focused on the stability of the external walls at the ground level (Figs. 1c, 1d) since their failure might lead to the collapse of the supported walls and floors. The behavior of each reference wall will depend on the characteristics of the wall itself, on its relation with the surrounding walls, on

the intensity of the flood action, and on the possible masonry failure mechanisms. Each reference wall (Fig. 2a) is characterized by width l (m), thickness t (m), and interstorey height Z (m). The wall is assumed to be impacted by a flood with density ρ_f (kg m^{-3}) rising up to a maximum level h_{max} (m). The wall is subject to a uniformly distributed vertical load per unit length, which is a function of the number of the upper floors and the geometrical characteristics of the walls. The self-weight of the masonry blocks is represented by the dead load resultant, which is applied at the centroid of the block.

The response of the wall to the force exerted by the flow depends on the efficiency of the constraint provided by the cross-walls, the floor, and the foundation (dashed red lines in Figs. 2b to 2e). Four conditions can be identified, namely P1 (Fig. 2b), P2 (Fig. 2c), P3 (Fig. 2d), and P4 (Fig. 2e). Wall P1 is simply supported at the foundation level (1-edge support), wall P2 is simply supported at the top and at the foundation level (2-edges support), wall P3 is simply supported on the cross-walls and at the foundation level but it is devoid of constraint at the top along the floor line (3-edges support), and wall P4 is simply supported along its perimeter by the cross-walls, at the top and at the foundation level.

Walls P1 and P2 are particular conditions of walls P3 and P4, respectively. Indeed, anytime the cross-walls feature wide openings close to the intersections with the wall impacted by the flow, the effectiveness of the restraint provided by the cross-walls is jeopardized. In addition, if the cross-walls spacing increases, the cross-wall constraining effect progressively reduces at the midspan. Therefore, P1 can be considered as an asymptotic representation of P3 when the wall aspect ratio increases, analogously P2 with P4.

2.1 Flood load model

Several contributions in the literature [e.g., *Zanuttigh and Lamberti*, 2006; *Armanini*, 2009] have experimentally computed the impact force on an obstacle with respect to the features of the upstream undisturbed flow of depth h (m) and mean velocity U (m s^{-1}). Other experimental models [e.g. *Cross*, 1967] provide empirical formulas for the impact force per unit width f (N m^{-1}) based on the total force of a 1D current where the dynamic term is amplified by a coefficient C_F (-), as:

$$f = \frac{1}{2} g \rho_f h^2 + C_F \rho_f h U^2 \qquad (1)$$

where ρ_f (kg m^{-3}) is the fluid density and g (m s^{-2}) is the gravity acceleration.

Experimental tests performed by *Armanini et al.* [2011] showed that the impact of the flow

against an obstacle generates a run-up h_{max} (m) in correspondence of the obstacle that can be related and computed from the features (e.g. Froude number, Fr) of the undisturbed flow upstream. The run-up shows up as a positive backward wave in case of subcritical flows or as a vertical jet in case of supercritical flows. Accordingly, the force per unit width exerted by the flow on an infinitely stiff vertical wall could be computed as the integral of the pressure profile p (Pa) on the impacted wall:

$$f = \int_o^{\min(Z,h_{max})} p\, dz \qquad (2)$$

Armanini et al. [2011] considered the case of an obstacle that intersects the whole cross section of a flume. In this extreme situation where the obstacle can't be surrounded by the flow, they showed that, in case of subcritical flow, good results can be obtained under the assumption of hydrostatic pressure distribution. When the incoming flow is supercritical, the pressure distribution differs from the hydrostatic one, with lower values on the upper part of the distribution and greater values at the bottom. Accordingly, they computed the impact force by introducing a corrective factor depending on the Froude number of the undisturbed flow.

Aureli et al. [2015] experimentally studied the 2D flow field around an isolated building, placed in a wide rectangular domain with horizontal bottom, caused by a sudden dam break generated by the opening of gate placed in the middle of a wall that separates a reservoir (located upstream and initially filled with still-water) from the downstream floodplain. The flow in front of the obstacle is characterized by Fr ≈ 3. The measured impact force was compared to the estimates of three different numerical models (i.e. the 2D depth-averaged Shallow Water Equations (SWE), a 3D Eulerian two-phase model, and a 3D Smoothed Particle Hydrodynamics (SPH) model). Using the results from a 2D SWE solver, *Aureli et al.* [2015] computed the maximum force on the obstacle, with a close fit to the measurements.

In this research a 2D SWE solver based on the numerical scheme proposed by *Braschi and Gallati* [1992] was implemented (in the following identified as 2D BG) and applied to the test case of *Aureli et al.* [2015] (Figs. 3a to 3f). On the obstacle wall a *free slip* condition was considered. The force on the building was computed by integrating at each time step the pressure distribution on all the mesh elements adjacent to the wall. The temporal trend of the computed force was positively compared with the numerical and experimental results of *Aureli et al.* [2015] (Fig. 3g).

According to these results and to the mentioned literature studies, in spite of the absence of

vertical acceleration, 2D SWE models provide an error in the peak force in the order of 10% with respect to the experimental data. Thus, in the following the force exerted by the flow on the wall can be computed hydrostatically as a function of the maximum run-up height during the impact that can operatively be obtained by solving the 2D SWE in the flooded domain of interest.

2.2 Finite Element analyses

To address the typical collapse mechanisms of exposed walls, detailed numerical FEM analyses were carried out. The model of a reference wall was developed in Abaqus (ver. 6.11, 2011) adopting 8-node brick elements (C3D8) and studied by changing boundary conditions at the side edges and at the top edge on the 4 wall types (Figs. 2b to 2e). A reference wall 3 m high (Z), 6 m long (l), and 0.3 m thick (t) was considered. The mechanical characteristics of a historic brick masonry of average quality were assumed [e.g., *Hilsdorf*, 1969; *Cominelli et al.*, 2016; *Page* 1981 and 1983]: masonry density ρ_m=1800 kg m^{-3}, elastic modulus E=3000 MPa, Poisson ratio 0.2, compressive strength f_c=3 MPa, tension strength f_t=0.03 MPa, fracture energy E_f=0.055 kJ m^{-2}, dilation angle Φ_d=20°. The masonry was treated as a homogeneous material as conventionally done in macro-modeling [e.g., *Lourenco*, 1996; *Milani et al.*, 2006a and 2006b] and the built-in model for concrete available in Abaqus was used. A smeared crack model (as opposed to a discrete crack model) is adopted to describe the masonry fracture process. Such model, referred to as "concrete damage plasticity", provides a general capability for modeling quasi-brittle materials in various types of structures, including concrete and masonry, when subjected to monotonic, cyclic, or dynamic loading. The failure stress corresponds to the onset of micro-cracking, beyond which further micro-cracks development is represented macroscopically with a softening stress-strain response inducing strain localization. In the particular case of masonry wall panels, the adopted model strategy provides an approximation of the actual structural behavior because it cannot capture the preferential crack path that could develop at the masonry joints. The boundary conditions were applied as surface restraints; in particular, translational restraints along the x, y, and z directions (Fig. 2a) at the bottom surface (i.e. at the foundation level) and translational restraints along the transversal direction (i.e. y in Fig. 2a) at the lateral and top surfaces. The mesh size was selected in order to subdivide the thickness of the wall panel into 4 slices and to get roughly cubic brick elements.

These analyses considered only the self-weight of the impacted walls; the effects of the vertical loads from the upper floors will be considered in the following sections. The analyses were

conducted in two subsequent steps: in the first step the gravity load is applied; in the second step the hydrostatic pressure is added, considering a water density equal to 1000 kg m^{-3}. Several analyses were carried out on each reference wall by increasing the impact flow depth. The minimum height h_{max} inducing the failure of the wall (i.e the maximum admissible water depth bearable by the wall) was recorded. The "Static-Riks" [*Dassault Systèmes Simulia*, 2011] type of analysis was selected for the loading increment procedure. This type of analysis uses an arc-length method to determine the response of the loaded structure and it is particularly suitable when a significant change of the structural stiffness is expected.

Figures 4a to 4d show the deflected shape of the models at failure along with the location of the tensile plastic strains, representing the zones where major cracks are triggered. It is worth noting that the chosen model strategy allows identifying the crack pattern associated with the initiation of the failure mechanism, herein referred to as "failure" in general terms. It is assumed that the development of the complete mechanism follows the same pattern. The failure of reference wall P1 (Fig. 4a) can be schematized as the rotation of the entire wall along the hinge at the foundation level after the development of a fracture line. The addition of the constraint at the floor level in case P2 (Fig. 4b) generates an out-of-plane deflection of the wall that rotates around the horizontal cylindrical hinges at the base, at the top, and at an intermediate distance from the ground. Similarly to case P1, in case P3 (Fig. 4c) the wall can displace at the top but the constraints guaranteed at the foundation level and by the cross-walls generate three hinges on the boundary of the wall and two internal hinges connecting the bottom corners to the upper edge of the wall. These fracture lines split the wall in three blocks that can rotate around them. Finally, in case P4 (Fig. 4d) all the sides of the wall have constraints and the out-of-plane deflection triggers 5 internal fracture lines that limit the blocks of the wall and allow their rotation. Figure 4e shows the results in terms of flood load versus maximum out-of-plane deflection (d). For the considered reference walls, the flood heights h_{max} causing the collapse of the walls (herein taken as the initiation of the failure mechanism corresponding to the maximum lateral load) are 1.14 m, 1.40 m, 1.30 m, and 1.57 m for the P1, P2, P3, and P4 reference walls, respectively. As expected, the flood load associated with the wall collapse increases as the degree of restraint of the wall sides increases (i.e. the values for P2 and P4 are greater than the corresponding values for P1 and P3, respectively).

2.3 Limit Analysis – main assumptions

As outlined above, FEM analyses provide detailed results that however depend on a large set of reliable parameters and require large computational efforts. The combination of these

necessary requirements suggests that, especially for application on large building stocks, detailed numerical analyses are in most cases unfeasible because of the unavailability of the requested data and of the required computational resources. To this purpose, after the detection of the main collapse mechanisms affecting a wall impacted by a flow, a simpler evaluation of the flood height causing wall failure is specifically proposed. Differently from existing strategies to evaluate building vulnerability based on numerical analyses [e.g., *De Risi et al.*, 2013], this task is accomplished herein by means of limit analysis considering the reference walls in Fig. 2 and the failure mechanisms highlighted in Figs. 4a to 4d.

Limit analysis is commonly addressed for the assessment of the structural behavior of masonry walls of good quality [e.g., *Milani et al.*, 2006b; *Como*, 2016]. Reference to local failure mechanisms is common practice in the case of historical masonry buildings, particularly for the assessment of the response of walls subject to transversal actions, such as those associated with an earthquake [*D'Ayala and Speranza*, 2003; *Italian Building Code*, 2008; *Giuriani and Marini*, 2008] and, for analogy, with the impact load of floods.

When the flood pressure exceeds the limit value (i.e. the hydrostatic pressure associated with h_{max}), the masonry wall impacted by the flood experiences the onset of a failure mechanism. Given the assumption of average/good quality masonry, the wall is assumed to split into monolithic blocks identified by a series of possible fracture lines. Each block rotates about the cylindrical hinges developing along the fracture lines (dashed blue lines in Figs. 2b to 2e), whereas no relative slip among adjacent blocks is considered.

A summary of the main assumptions underlying the analysis is:

- unlimited compressive strength and stiffness of the masonry;
- no tensile resistance of the masonry;
- no slip occurring between masonry elements;
- quality of the masonry sufficient as to allow homogenization;
- no scour effects at the foundation level.

Focusing on flash flood processes, we assume that the flood action cannot be counteracted by a pressure distribution at the inner side of the wall since the time needed for the filling of the internal volume is much greater than the characteristic time of the impact. For the same reasons, the physical loss of material volume and change in the material mechanical properties, which could be triggered only by an extended period of contact with water, are not considered.

2.4 Limit analysis - Description of the model

The collapse mechanisms and their stability thresholds are studied by using the principle of virtual works and within the limit analysis framework, that is, with the hypothesis of infinite compressive resistance and stiffness of the masonry and hence neglecting the internal work along the fracture lines. Accordingly, only the work done by the external forces is considered at this stage. The stability threshold, i.e. the onset of the failure mechanism, is achieved when the absolute value of the work done by the stabilizing actions (L^+) equals the absolute value of the work done by the overturning actions (L^-):

$$\frac{L^+}{L^-} = 1 \qquad (3)$$

As discussed in Section 2, the reference walls P1 and P2 can be considered sub-cases of the walls P3 and P4, respectively. Accordingly, only the limit analysis of the reference wall P3 (i.e. 3-edges support) and P4 (i.e. 4-edges support) is presented in the following.

In the reference wall P3 (Fig. 5), the failure mechanism considers the onset of 2 internal fracture lines splitting the wall in 3 blocks. The central block rotates around the cylindrical hinge at the ground level and the two side blocks, delimited by inclined fracture lines, rotate around the vertical hinges at the sides of the wall. It is worth noting that the model does not guarantee the compatibility along the vertical fracture lines; the minor impact of such a simplified assumption is assessed by nonlinear finite element analyses in the Section 4.

The stabilizing contribution is provided by the self-weight of the three blocks in which the wall is divided and by the load per unit length n (N m^{-1}) applied along the center line of the top face of the wall, replicating the dead load of the upper floors. The central block of the wall is subject to a vertical (in direction z) displacement $\xi_1 = t/2 \cdot \vartheta_1$ smaller than the displacement $\xi_3 = t \cdot \vartheta_1$ experienced by the side blocks assuming that the hinge lines develop along the outer edges of the wall. The external loads $N_1 = n \cdot l_c$ (N) and $N_3 = n \cdot l_s$ (N), applied along the central and lateral blocks upper edges respectively, depends on the tributary portion of the wall that is defined on the top by l_c and l_s (Eq. 5). In these scheme the external loads are applied at the centroid of the cross section, thereby experiencing vertical displacements $\xi_{N1} = t/2 \cdot \vartheta_1$ and $\xi_{N3} = t \cdot \vartheta_1$. The work done by the stabilizing actions is obtained from summing the products between the gravity loads and the corresponding vertical displacements:

$$L^+ = W_1\xi_1 + 2W_3\xi_3 + N_1\xi_{N1} + 2N_3\xi_{N3} = (W_1 + N_1)\frac{t}{2}\vartheta_1 + 2(W_3 + N_3)t\vartheta_1 \quad (4)$$

l_s (side block width at the top) and l_c (central block width at the top) are respectively:

$$l_s = Z\tan\alpha;\ l_c = l - 2l_s \quad (5)$$

It is worth noting that the virtual vertical displacements ξ_i are obtained directly from the hypothesis of small deflections (i.e. small ϑ_i). In such conditions $\operatorname{sen}\vartheta_i$ and $\tan\vartheta_i$ can be approximated with the first order of the Taylor series (i.e. ϑ_i, expressed in radians).

The work done by the external overturning action due to the flow pressure $p(z)=\rho_f g(h_{max}-z)$ is evaluated by considering the load share acting on the central block, undergoing a rotation ϑ_1 with respect to the wall lower edge, and on the lateral blocks, subjected to a rotation ϑ_3 with respect to the lateral edges (Fig. 5b). The fracture lines develop with an angle α (°) with respect to the vertical cross-walls. Equating the lateral displacements of two adjacent blocks at their intersection at a height z we obtain:

$$\vartheta_1 z = \vartheta_3 z\tan\alpha \rightarrow \vartheta_3 = \frac{1}{\tan\alpha}\vartheta_1 \quad (6)$$

The work done by the external overturning action is:

$$L^- = \int_0^{\min(h_{max},Z)} pl_1\delta_1 dz + 2\int_0^{\min(h_{max},Z)} pl_3\delta_3 dz = \int_0^{\min(h_{max},Z)} pl_1 z\vartheta_1 dz + 2\int_0^{\min(h_{max},Z)} p\frac{{l_3}^2}{2}\vartheta_3 dz \quad (7)$$

Subscripts 1 and 3 represent the central and side blocks, respectively, and are associated with the displacements δ in direction y of the application points of the infinitesimal hydrostatic forces at distance z from the ground. Considering each side block, the application point is located horizontally at a distance $l_3/2$ from the lateral hinge. The terms l_1 and l_3 are the lengths of the central and lateral blocks respectively computed at level z as a function of α:

$$l_3 = z\tan\alpha;\ l_1 = l - 2l_3 \quad (8)$$

At the top edge, l_1 and l_3 correspond to l_c and l_s, respectively. The numerical solution of Eq.3 yields the minimum depth of the flood that triggers the failure mechanism of the wall h_{max} (i.e. the maximum admissible water depth before the wall collapse).

The reference wall P1 can be considered a particular case of the configuration P3 in case the

cross-walls do not provide any support. In this case, the whole panel experiences the overturning along the foundation line and no onset of any inclined fracture line can be observed. Accordingly, this situation can be modeled considering that the behavior of the central block coincides with the overall wall. As a result, the second integral of the work of the destabilizing forces is nil. In other terms the vulnerability analysis of reference wall P1 can be obtained from replacing α=0° and ϑ_3=0° in the previous expressions. In the case α causes the intersection of the skewed fracture lines inside the wall, a slightly different failure mechanism producing a vertical fracture line can be observed as discussed in detail in the Appendix.

Considering the reference wall P4 (Fig. 6), the failure mechanism considers the onset of 5 internal fracture lines splitting the wall in 4 blocks. Two overlying central blocks, divided by a horizontal hinge at distance h_c (m) from the ground, rotate around three cylindrical hinges at the top, at h_c, and at the ground. Two side blocks delimited by inclined fracture lines rotate around the vertical hinges at the sides of the wall. As in the previous case, compatibility along the vertical fracture lines is not guaranteed. The effect of this assumption is discussed in Section 4.

The stabilizing contribution is provided by the self-weight of the blocks in which the wall is divided and by the dead load N of the upper floors. Regarding the position of the vertical load N, it is worth observing that a horizontal fracture line develops at the floor level and the vertical load migrates to the side. In such a case, under the hypothesis of infinite compressive resistance and stiffness of the masonry, we applied the vertical load at the wall corner in the limit analysis. On the contrary, in the reference wall P3 (Fig. 5), the vertical load N is centered because no horizontal fracture line develops at the floor level.

The lower central block, of weight W_1, and the lateral ones, of weight W_3, are associated with different vertical displacements in direction z ($\xi_1 = t/2 \cdot \vartheta_1$ and $\xi_3 = t \cdot \vartheta_1$, respectively) related to the rotation angle ϑ_1 only, while the vertical displacements of the upper central block of weight W_2 ($\xi_2 = t \cdot \vartheta_1 + t/2 \cdot \vartheta_2$) and of the center of application of the external vertical load N ($\xi_N = t \cdot \vartheta_1 + t \cdot \vartheta_2$) are functions of both ϑ_1 and ϑ_2. The work done by the stabilizing actions can be computed as:

$$L^+ = W_1\xi_1 + W_2\xi_2 + 2W_3\xi_3 + N\xi_N$$
$$= W_1\frac{t}{2}\vartheta_1 + W_2\left(t\vartheta_1 + \frac{t}{2}\vartheta_2\right) + 2W_3 t\vartheta_1 + N(t\vartheta_1 + t\vartheta_2) \quad (9)$$

The work done by the external overturning hydrostatic action is evaluated, following the same

approach presented in the previous scheme, considering that the load share on the different blocks depends on their width l_1, l_2, and l_3 at level z:

$$\begin{aligned} L^- &= \int_0^{\min(h_{max},h_c)} pl_1\delta_1 dz + \int_{\min(h_{max},h_c)}^{\min(h_{max},Z)} pl_2\delta_2 dz + 2\int_0^{\min(h_{max},Z)} pl_3\delta_3 dz \\ &= \int_0^{\min(h_{max},h_c)} pl_1 z\vartheta_1 dz + \int_{\min(h_{max},h_c)}^{\min(h_{max},Z)} pl_2(Z-z)\vartheta_2 dz \\ &+ 2\int_0^{\min(h_{max},Z)} p \quad \frac{{l_3}^2}{2}\vartheta_3 dz \end{aligned} \tag{10}$$

where

$$l_3 = \begin{cases} z\tan\alpha \ \ if\ z < h_c \\ (Z-z)\tan\beta \ if\ z > h_c \end{cases} \tag{11}$$

$$l_1 = l - 2l_3;\ l_2 = l - 2l_3 \tag{12}$$

$$\beta = \tan^{-1}\left[\left(\frac{h_c}{Z-h_c}\right)\tan\alpha\right] \tag{13}$$

As in the previous scheme, the numerical solution of Eq. 3 yields the minimum depth h_{max} of the flood that triggers the failure mechanism of the wall. Such depth also determines the location h_c of the horizontal fracture line, which is taken as the minimum among its possible locations: indeed, the proposed model does not account for the internal work at the fracture lines, therefore more patterns of fracture lines could be possible for the same value of h_{max}. If the horizontal fracture line is above the maximum run-up, the second integral of Eq. 10 is nil.

The reference wall P2 can be considered a sub-case of P4 due to the absence of lateral restraint from the cross-walls. In this case, only the horizontal fracture line at h_c can be observed and the wall decomposes in two blocks that rotates around the three horizontal hinges at the ground level, at h_c, and at the floor level. As in the previous case, the stability of the reference wall P2 can be operatively modeled by replacing $\alpha = 0°$ and $\vartheta_3 = 0°$ in the previous expressions.

In limit analysis α is usually obtained from an energy minimization procedure. Anyway, as mentioned before, the present simplified model disregards the contribution of internal works developed at the block interfaces since it would require detailed data on the mechanical properties of the materials and their state of conservation. Accordingly, in this case the

assessment of α based on the energy minimization would lead to α=0°, that is contrary to the observations in the practice. Indeed, in-field surveys of masonry walls subjected by out-of-plane inertial loads (e.g. seismic) show α between 0° and 40°. In order to cope with the need of suggesting reliable values of α for the application of the model, in Section 3 a set of possible values for the angle under different wall configurations is provided from the results of FEM analyses performed assuming average masonry properties.

2.5 Dimensional analysis

In order to cast the analysis in a more general framework and to reduce the complexity arising from the presence of several variables, the results must be proposed in dimensionless form. Considering the assumptions on the characteristics of the materials at the base of the proposed model, the dimensionless ratio of the work done by the stabilizing (L^+) and overturning (L^-) actions, can be written, for each reference scheme (P1 to P4), as a functional relation of n=8 independent variables:

$$\frac{L^+}{L^-} = f\left(g, \rho_m, l, t, Z, n, h_{max}, \rho_f\right) \tag{14}$$

Applying the Buckingham theorem to Eq. 14 and assuming as basic quantities with independent dimensions [e.g. *Yalin*, 1977] g, ρ_m and Z (i.e. k=3) it is possible to obtain n-k=5 dimensionless groups:

$$X_1 = \frac{l}{Z}$$ Wall aspect ratio

$$X_2 = \frac{t}{Z}$$ Slenderness of the wall

$$X_3 = \frac{n}{\rho_m g Z t}$$ Ratio between load at the top of the wall and wall weight

$$X_4 = \frac{h_{max}}{Z}$$ Fraction of wall impacted by the flow

$$X_5 = \frac{\rho_f}{\rho_m}$$ Ratio between fluid and masonry density

All the parameters, except X_4 and X_5, represent the geometry of the wall and its relationship with the other structural elements of the building. The parameter X_3, that is the ratio between the vertical loads and the weight of the impacted wall, represents the number of floors above the ground floor under the hypotheses of non-tapered walls and negligible loads on the floors. These assumptions will be maintained in the following. Finally, the dimensionless number X_4 represents the maximum admissible water depth (i.e., h_{max}) at the wall before the collapse, thereby providing a measure of its vulnerability. Although the inclination α of the lateral blocks in schemes P3 and P4 is considered an input parameter in our simplified model, it is itself a function of X_1 and X_3 as discussed in the following section. Accordingly, the angle α is not accounted among the independent variables in Eq. 14.

3. Results and comparison with FEM simulations

The equations described in Section 2.4 representing the different collapse mechanisms have been solved in correspondence of a wide range of the dimensional variables and the results have been rewritten in dimensionless form in order to simplify the application of the model. The resulting dimensionless curves related to the different support schemes are reported below (Fig. 7) as functions of the wall slenderness X_2 and of the vertical fraction of wall impacted by the flow X_4. All the thresholds in Figs 7a to 7d were computed considering the case of a water flow (ρ_f= 1000 kg m^{-3}) impacting a wall of average density ρ_m =1800 kg m^{-3} leading to X_5=0.56. The stability curves were derived considering the values of α reported in Tab. 1. Such values were obtained from nonlinear FEM analyses, similarly to what presented in Section 2.2 and represent the mean value obtained for slenderness of the wall (X_2) in the range 0.1-0.2 (relative error less than 7%). In the reference wall P3, it is interesting to note that α decreases when the vertical load increases if X_1=2, while, for X_1=1, α is constant and the failure mechanism is the one reported in the Appendix. In the P4 case, α is roughly constant given the wall shape factor (X_1). It is worth to remember that, according to the chosen modeling strategy, the values of α are associated with the initiation of failure and do not capture possible preferential crack path at the masonry joints.

The stability curves were computed for buildings of up to 2 floors over the ground floor (i.e., X_3=[0,1,2]), wall aspect ratio X_1 =[1,2] (linear regression could be adopted for intermediate values of X_1) and slenderness X_2=0.05÷0.35. It is worth noting that for cases P1 and P2, the model can be written considering a strip of unit width, disregarding the width l of the wall. Accordingly, the resulting thresholds are independent from the dimensionless group X_1 and Figs. (7a and 7b) show a single curve for each external load configuration (i.e., X_3). For clarity

of representation, the water depth was considered ranging from 0 to 2Z (X_4=0÷2) only in order to consider floods causing maximum run-up up to the second floor. In the case of buildings without upper floors (X_3=0), the limit of validity of the model is X_4=1.

As expected, the resulting dimensionless thresholds show a general increase of stability (i.e. dimensionless maximum admissible water depth X_4) for increasing dimensionless thickness (X_2) of the wall and increasing vertical loads (X_3). The stability curves of reference walls P3 and P4 are characterized by higher values compared to P1 and P2, respectively. Moreover, an increase of the wall aspect ratio X_1 for the reference walls P3 and P4 corresponds to a decrease in the resistance since the cross-walls influence area progressively reduces to a small fraction of the entire wall and the effectiveness of their restraining action diminishes. Generally, the reference wall P4 (4 edges-support) is characterized by higher stability limits compared to P3 (3-edges support).

The model can be adapted to represent different masonry materials and processes characterized by density higher than water. For instance, as discussed by *Milanesi et al.* [2014 and 2015], disregarding the concentrated impacts of debris but focusing on the case of hyperconcentrated flows, one might observe that the increase of fluid density is mostly due to the presence of suspended sediment, so that the fluid is still mono-phasic and the mechanistic vulnerability model is still valid. Accordingly, although the model is not able to cope with the highly complex challenge of debris impacts it provides a simplified and rational approach to describe the interaction between a mudflow and a structure. Figs. 7e to 7h, computed for $0<X_3<2$ and X_1=2, show that the increase of the ratio X_5 (i.e. an increase of the equivalent homogeneous flow density) leads to a general decrease of the dimensionless maximum admissible flow depth X_4.

The stability thresholds obtained from the limit analysis approach under the mentioned simplifying assumptions were compared with the results of nonlinear numerical analyses (FEM) carried out on the same models presented in Section 2.2 by varying the wall thickness (thickness values ranging from 0.3 m to 0.75 m, leading to X_2 between 0.1 and 0.25) and the number of floors (only the self-weight of the wall, i.e. X_3=0, and 2 floors above the ground floor, i.e. X_3=2). The other dimensionless variables of the considered case study were: wall aspect ratio X_1=2 and ratio between fluid and masonry density X_5=0.56 (ρ_m=1800 kg m^{-3} and ρ_f=1000 kg m^{-3}). The comparison of the result of the FEM analyses with the thresholds from the simplified approach provides a benchmark for the proposed approach and especially for the reliability of the simplifying assumptions discussed in Section 2.3. The resulting minimum heights h_{max} causing failure of the walls are plotted in dimensionless terms (X_4) as solid dots in

Figs. 7a to 7d showing good agreement with the thresholds (dashed lines, X_1=2) of the conceptual simplified model for all the considered support schemes and loading conditions. Similarly, a positive comparison of the dimensional values of the hydrostatic force at failure (i.e. at the initiation of the mechanism) obtained with the FEM model and the limit analysis is proposed in Fig. 4

4. Discussion

The proposed model is based on a set of assumptions, whose reliability was tested with the numerical FEM analyses. For instance, in order to provide a better representation of the process, the compression strength of the material could have been accounted in the model. In this case, the pivot points would be represented by areas of finite dimension defined as the ratio between the vertical force and the compressive strength f_c (N m^{-2}) of the material. This parameter, included in the right-hand side of Eq. (14), would lead to the dimensionless group X_6 that is the ratio between the compressive strength of the masonry and the pressure at the base of a single floor wall:

$$X_6 = \frac{f_c}{\rho_m g Z} \qquad \text{Dimensionless compressive strength}$$

The introduction of the compressive strength in the model would cause the in-ward shift in the pivoting hinges, increasing the vulnerability of the impacted wall. However, the FEM simulations showed that this improvement has a negligible effect in the estimation of the flood height h_{max} at failure.

A sensitivity analysis on the FEM results was carried out to further highlight the influence of the mechanical parameters related to masonry stiffness and strength. This analysis was performed on the reference walls tested with the FEM model by halving and doubling the elastic modulus, the compressive strength and the tensile strength of the masonry. For demonstration purposes, the analysis of the reference wall P2 with and without additional loads at the top is shown in Tab. 2. The results are presented as percent variations with respect to the dimensionless critical depth X_4 computed for the reference case study.

The sensitivity analysis confirmed that the variation of the compressive strength and stiffness marginally affects the results of the proposed model. The tensile strength (f_t) of the masonry is

the parameter which mostly affects the results, with variations below 10%. In particular, increasing or decreasing the tensile strength led to an increase or a decrease of the critical flood depth, respectively. The variation of the other parameters led to smaller changes of the results. Other simplifications were introduced in the crucial phase of the selection of boundary conditions. At the base of the wall, all the translational degrees of freedom of the nodes at the wall-foundation interface were fixed; in addition, no scour effects were considered and possible erosion in correspondence of the cement mortar layers was neglected. These limitations also characterize the other empirical vulnerability functions available in the literature [see *Papathoma-Köhle et al.*, 2017 for a discussion] and allowed to consider the wall as monolithic. Considering these details would require further information on the foundations and on the quality and conservation of the masonry. On the sides of the wall, cylindrical hinges were assumed, as reasonable in the case of a modest brick/stone texture and limited mutual interlocking.

The selection of the most adequate reference model (P1 to P4) depends on the transversal constraints at the top of the wall and on the presence, connections and orientation of cross-walls. The lack of support along the upper edge of the impacted wall may be the result of the presence of the stairwell or may be due to orientation of the floor joists or roof rafters (in case the joists are parallel to the wall, no constraint is provided to the wall); in this case schemes P1 or P3 should be selected. Similarly, if cross-walls have significant openings (e.g. doors or windows) in correspondence to the edges, their restraining effect on the wall lateral sides is negligible, and schemes P1 or P2 should be selected.

In this simplified vulnerability model, the presence of openings on the impacted wall can be accounted for in a conservative way by considering only the portions of the wall adjacent to the opening (door or window) and the reference conditions P1 or P2, depending on the out-of-plane restraint at the top of the wall.

As mentioned in Section 2.4, in case of increasing wall aspect ratio, the reference walls P1 and P2 can be considered an asymptotical representation of walls P3 and P4 respectively. Indeed, the greater is the wall aspect ratio X_1 (i.e., for a given height of the wall, the greater is the distance between the cross-walls) the lower is the area of influence of the cross-walls. The difference between the thresholds corresponding to cases P1 and P3 and cases P2 and P4 becomes smaller than 10% for X_1 greater than 4 and 2.75, respectively.

An example of application of the wall vulnerability model can be given with reference to the buildings shown in Figs. 1c and 1d. Both buildings are along the left side of the stream in Fig. 1a and 1b and their most exposed faces are free of relevant openings and with full support from

the cross-walls. The building in Figs. 1c and 8a has two floors so that the ground level supports the vertical weight of the upper floor and wall and of the roof. In a conservative way, only the weight of the upper wall will be considered. Given the geometry and under the assumption of non-tapered walls, the dimensionless vertical load X_3 ranges between 1 and 1.4 depending if the tympanum below the roof is considered. In order to assess the safety of the overall building, the stability of each single wall at the ground level must be considered. Under the assumption of the presence of an internal intermediate transversal wall and of horizontal slabs between the floors, the overall exposed wall could be considered composed by 4 smaller walls and the reference wall could be modeled according to the 4-edges support scheme (P4). The overall building is about 8 m wide and accordingly the width l of each reference wall is 4 m. The wall aspect ratio $X_1 \approx 1.6$ leads to Z=2.5 m. By estimating a thickness t=0.55 m, the slenderness of each single wall is X_2=0.22. Given these assumptions on the organization of the structure and on the geometrical input data, the stability limit is reached for a maximum water depth in the range $1.8<X_4<2$, depending on the considered vertical load (Fig. 8a). Moreover, an increase of the fluid density up to ρ_f=1500 kg m^{-3} (X_5=0.83) or ρ_f=2000 kg m^{-3} (X_5=1.11) would reduce the maximum admissible water depth in the range $1.40 <X_4< 1.60$ or $1.15 <X_4< 1.30$, respectively. Figures 1d and 8b shows a single floor building, where the vertical dimensionless load could be considered in the range $0<X_3<0.2$ if the weight of tympanum is included. Assuming the absence of a horizontal slab and the presence of an intermediate internal cross-wall, the overall exposed wall (8 m wide) can be decomposed in two single walls to be studied using the 3-edges support scheme (P3) since no relevant openings on the cross-walls are present. Considering a wall aspect ratio X_1=1.2, l=4 m, Z=3.3 m, t=0.5 m, and a slenderness X_2=0.15, the resulting stability limit lies in the range $0.60<X_4<0.65$ (Fig. 8b). As shown in the previous test-case, an increase of the relative density to X_5=0.83 and X_5=1.11 would lead to an overall increase of vulnerability in the range $0.5<X_4<0.55$ and $0.45<X_4<0.50$, respectively.

5. Conclusions

In mountain hazards risk management, the assessment of the structural vulnerability of buildings exposed to flash floods is an important and challenging task. In recent years, multiple approaches using empirical vulnerability functions [e.g., *Papathoma-Köhle et al.*, 2012; *Totschnig and Fuchs*, 2013; *Totschnig et al.*, 2011], matrices [e.g., *Hu et al.*, 2012; *Zanchetta et al.*, 2004] and indicators [e.g., *Ettinger et al.*, 2016; *Thouret et al.*, 2014] have been published and discussed as appropriate methods to increase the overall explanatory power of risk

assessment. However, the interactions between elements at risk and the hazard processes have been largely ignored. Consequently, the necessary information for operational hazard and risk mitigation has not been adequately defined [*Mazzorana et al.*, 2012; *Mazzorana et al.*, 2014; *Papathoma-Köhle et al.*, 2017].

This paper showed that the necessary results depend on a detailed knowledge of the interaction between the flow and the impacted structures. In spite of the social and economic relevance of this topic, with respect to mountain hazards few viable and reliable approaches are documented in the literature [e.g., *Armanini et al.*, 2011; *Gems et al.*, 2016; *Mazzorana et al.*, 2014].

The response of a structure to a given flow impact is determined by the building technology, the materials and the configuration of the building itself, inhibiting the search for a general solution. Moreover, the required detail and accuracy depend greatly on the purpose of the study and on its scale (e.g., land planning, building design, etc.). Accordingly, a physically-based model should incorporating these aspects and detailed numerical analyses (e.g., through FEM) would seem to be the most ideal method to tackle this issue. However, detailed approaches are not feasible in case of studies on large buildings stocks due to the quantity and reliability of required data and the necessarily large computational resources. Often the goal of these studies is to single out the most exposed buildings [*Kienholz et al.*, 2004] to be further investigated with more advanced approaches or adaptation [*Holub and Fuchs*, 2008; *Holub et al.*, 2012].

In order to obtain an economical and realistically achievable assessment, we proposed a simplified model for a physically-based estimate of the vulnerability to flash floods for masonry buildings, typical of mountain areas, that couples limit analysis with flood hazard data obtained via hydraulic modeling. The model conceptualizes the failure mechanism by employing simplified geometric data and general information on the global layout of the structure. This makes the approach practical for operational vulnerability assessment. In the absence of experimental and field data, the stability results provided by the model were positively compared with the numerical results of an advanced FEM analyses and reorganized in dimensionless fashion, so that they can be easily applied to general situations. At the current stage, only the vulnerability associated with the initial impact of a flash flood is considered.

Due to the limited amount of data required for this model, and the direct availability of such information through field surveys, the model is particularly suitable for analysis on large building stocks, as is usual for a first vulnerability estimate in the field of earthquake engineering. As such, the approach can be adopted for building retrofitting and land use planning in order to arrive at more resilient mountain societies, one of the goals specified in the Sendai Framework for Disaster Risk Reduction [*Zimmermann and Keiler*, 2015]. The

methods presented in this paper can be further used to better validate the skew of empirical vulnerability functions [*Papathoma-Köhle et al.*, 2015], and to better understand building-specific damage-generating mechanisms in the European Alps [e.g. *Fuchs et al.*, 2007; *Totschnig and Fuchs*, 2013] and beyond [e.g. *Jakob et al.*, 2012; *Lo et al.*, 2012].

In the future, the proposed model could be further developed, including the role of doors and windows, exploring the behavior of the overall building under time-varying impact loads, and defining other types of limit states (currently only wall failure was considered) as well as the economic implications of structural flood damages. Finally, a probabilistic approach accounting for the variability of materials, building technologies and model uncertainties could allow a quantification of collapse probability.

Acknowledgements

No new data were used in producing this manuscript. Sven Fuchs received funding from the Austrian Science Fund (FWF; P27400-NBL).

Appendix

This appendix presents the limit analysis of the reference wall P3 (i.e. 3-edges support) in the case the fracture lines intersects inside the wall panel (Fig. A1), which happens if the condition tan $\alpha > l/2Z$

is verified. The stabilizing contribution is provided by the self-weight of the three blocks in which the wall is divided and by the load per unit length applied along the center line of the top edge of the wall, replicating the dead load of the upper floors.

The central block of the wall of weight W_1 is subject to a vertical displacement $\xi_1 = t/2 \cdot \vartheta_1$ smaller than the displacement $\xi_3 = t \cdot \vartheta_1$ experienced by the side blocks of weight W_3 provided that the hinge line develops along the outer edge of the wall. The external vertical loads $N = n \cdot l$ are applied at the centroid of the cross section, thereby experiencing a vertical displacement $\xi_N = t \cdot \vartheta_1$. The work done by the stabilizing actions is:

$$L^+ = W_1 \xi_1 + 2W_2 \xi_3 + N\xi_N = W_1 \frac{t}{2} \vartheta_1 + (2W_3 + N) t \vartheta_1 \qquad \text{(A1)}$$

The work done by the external overturning action is evaluated by considering the load share acting on the central block, undergoing a rotation ϑ_1 with respect to the wall bottom edge, and on the lateral blocks, subjected to a rotation ϑ_3 (Eq. 6) with respect to the lateral edges (as in

Fig. 5).

$$L^{-} = \int_0^{\min(h_{max},Z)} pl_1\delta_1 dz + 2\int_0^{\min(h_{max},Z)} pl_3\delta_3 dz = \int_0^{\min(h_{max},Z)} pl_1 z\vartheta_1 dz + 2\int_0^{\min(h_{max},Z)} p\frac{{l_3}^2}{2}\vartheta_3 dz \quad \text{(A2)}$$

Subscripts 1 and 3, associated with the displacements δ in direction y and with the application points of the infinitesimal hydrostatic forces, represent the central block and the side blocks, respectively. The terms l_1 and l_3 are the lengths of the central and lateral blocks computed at level z as a function of α:

$$\begin{cases} l_3 = z\tan\alpha;\ l_1 = l - 2l_3\ if\ z < \dfrac{l}{2\tan\alpha} \\ l_3 = \dfrac{l}{2};\ l_1 = 0\ if\ z \geq \dfrac{l}{2\tan\alpha} \end{cases} \quad \text{(A3)}$$

References

Akbas, S., Blahut, J., Sterlacchini S., 2009. Critical assessment of existing physical vulnerability estimation approaches for debris flows. In: Malet, J., Remaître, A., Bogaard, T., editors. Landslide processes: From geomorphological mapping to dynamic modeling. CERG Editions, Strasbourgh, 229-233.

Alcrudo, F., and Mulet, J. 2007. Description of the Tous dam-break case study (Spain), Journal of Hydraulic Research, 45 (Extra Issue), 45–57, DOI: https://doi.org/10.1080/00221686.2007.9521832.

Alexander, J., Cooker, M. J. and Manville, V., 2016. Moving boulders in flash floods and estimating flow conditions using boulders in ancient deposits. Sedimentology, 63, 1582-1595. DOI:10.1111/sed.12274

Ancey, C., Iverson, R.M., Rentschler, M., Denlinger R.P., 2008. An exact solution for ideal dam-break floods on steep slopes. Water Resources Research, 44, W01430, DOI: https://doi.org/10.1029/2007WR006353.

Armanini, A., 2009. Discussion on: Experimental analysis of the impact of dry avalanches on structure and implication for debris flows by Zanuttigh, B. and Lamberti, A., Journal of Hydraulic Research, 44, 522–534, DOI: https://doi.org/10.1080/00221686.2009.9522009.

Armanini, A., Larcher, M., Odorizzi, M., 2011. Dynamic impact of a debris flow front against a vertical wall, in Proceedings of the 5th International Conference on Debris-Flow Hazards Mitigation: Mechanics, Prediction and Assessment, Padua, Italy, 1041-1049, DOI: https://doi.org/
10.4408/IJEGE.2011-03.B-113.

Arrighi, C., Alcèrreca-Huerta, J.C., Oumeraci, H., Castelli, F., 2015. Drag and lift contribution to the incipient motion of partly submerged flooded vehicles. Journal of fluids and structures, 57, 170-184, DOI: https://doi.org/10.1016/j.jfluidstructs.2015.06.010.

Aureli, F., Dazzi, S., Maranzoni, A., Mignosa, P., Vacondio, R., 2015. Experimental and numerical evaluation of the force due to the impact of a dam-break wave on a structure. Advances in Water Resources, DOI: http://dx.doi.org/10.1016/j.advwatres.2014.11.009.

Black, R., 1975. Flood proofing rural residences. A Project Agnes Report, Pennsylvania, Economic Development Administration, Washington DC.

Braschi, G., Gallati, M., 1992. A conservative flux prediction algo- rithm for the explicit computation of transcritical flow in natural streams, Proceedings Hydrosoft '92, Computational Mechanics Publications, Southampton, UK, 381–394.

Clausen, L., and Clark, P., 1990. The development of criteria for predicting dam break flood damages using modeling of historical dam failures, White, W. editor, Proceedings of the International Conference on River Flood Hydraulics, W. White, ed., Wiley, Chichester, U.K, 369–380.

Cominelli, S., Giuriani, E., Marini, A., 2016. Mechanisms governing the compressive strength of unconfined and confined rubble stone masonry. Mater Struct. 50:10, 1-14. DOI: https://doi.org/10.1617/s11527-016-0905-6

Como, M., 2016. Statics of Historic Masonry Constructions. Springer Verlag; Springer Series in Solid and Structural Mechanics. ISBN-10: 3319245678.

Costabile, P., Costanzo, C., Macchione, F., 2012. Comparative analysis of overland flow models using finite volume schemes, Journal of Hydroinformatics, 14(1), 122–135. DOI: 10.2166/hydro.2011.077.

Cross, R.H., 1967. Tsunami surge forces. Journal of the Waterways and Harbors Division, 93, 201-231.

Cuomo, G., Shams, G., Jonkman, S.N., van Gelder, P., 2009. Hydrodynamic loadings of buildings in floods,. Coastal Engineering 2008, Proceedings of the 31st International Conference, Hamburg, Germany, 31 August – 5 September 2008. DOI: https://doi.org/10.1142/9789814277426_0310.

Dale, K., Edwards, M., Middelmann, M., Zoppou, C., 2004. Structural flood vulnerability and the Australianisation of Black's curves, Proceedings of the Risk Conference, Risk Engineering Society, Barton, Australia.

Dassault Systèmes Simulia, 2011. Abaqus User's Manual Version 6.11, Providence, RI, USA.

D'Ayala, D., Speranza, E., 2003. Definition of collapse mechanisms and seismic vulnerability of masonry structures. Earthquake Spectra, 19(3), 479-509. DOI: https://doi.org/10.1193/1.1599896.

De Risi, R., Jalayer, F., De Paola, F., Iervolino, I., Giugni, M., Topa, M. E., Mbuya, E., Kyessi, A., Manfredi, G., Gasparini P., 2013. Flood risk assessment for informal settlements. Natural Hazards, 69, 1003-1032. DOI: https://doi.org/10.1007/s11069-013-0749-0

Di Baldassarre, G., Viglione, A., Carr, G., Kuil, L., Yan, K., Brandimarte, L., Blöschl, G., 2015. Perspectives on socio-hydrology: Capturing feedbacks between physical and social processes, Water Resources Research, 51, 4770-4781. DOI: https://doi.org/10.1002/2014WR016416.

Ettinger, S., et al. 2016. Building vulnerability to hydro-geomorphic hazards: Estimating damage probability from qualitative vulnerability assessment using logistic regression, Journal of Hydrology, 541(Part A), 541-563. DOI: https://doi.org/10.1016/j.jhydrol.2015.04.017.

Fuchs, S., Heiss, K., Hübl, J., 2007. Towards an empirical vulnerability function for use in debris flow risk assessment. Natural Hazards and Earth System Sciences, 7, 495-506, DOI: https://doi.org/10.5194/nhess-7-495-2007.

Fuchs, S., Keiler, M., Zischg, A., 2015. A spatiotemporal multi-hazard exposure assessment based on property data. Natural Hazards and Earth System Sciences, 15, 2127-2142, DOI: https://doi.org/10.5194/nhess-15-2127-2015.

Fuchs, S., Röthlisberger, V., Thaler, T., Zischg, A., Keiler, M., 2017. Natural hazard management from a coevolutionary perspective: Exposure and policy response in the European

Alps, Annals of the American Association of Geographers, 107, 382-392, DOI: https://doi.org/10.1080/24694452.2016.1235494.

Gems, B., Mazzorana, B., Hofer, T., Sturm, M., Gabl, R., Aufleger, M., 2016. 3-D hydrodynamic modelling of flood impacts on a building and indoor flooding processes. Natural Hazards and Earth System Sciences, 16, 1351-1361, DOI: https://doi.org/10.5194/nhess-16-1351-2016.

Giuriani, E., Marini, A., 2008. Experiences from the Northern Italy 2004 earthquake: vulnerability assessment and strengthening of historic churches. Invited paper. VI International Conference on Structural Analysis of Historical Constructions SAHC 2008. 2-4 July, Bath, England. pag. 13-24. Ed. Taylor and Francis, London, UK. ISBN 978-0-415-46872-5.

Guzzetti, F., Salvati, P., Stark, C., 2005. Historical evaluation of flood and landslide risk to the population of Italy. Environmental Management, 2005, 36, 15-36, DOI: https://doi.org/10.1007/s00267-003-0257-1.

Hilker, N., Badoux, A., Hegg, C., 2009. The Swiss flood and landslide damage database 1972-2007. Natural Hazards and Earth System Sciences, 9, 913-925, DOI: https://doi.org/10.5194/nhess-9-913-2009.

Hilsdorf, H.K., 1969, "Investigation into the failure mechanism of brick masonry loaded in axial compression", Designing, Engineering, and constructing with masonry products, Gulf Publishing Co., 34-41.

Holub, M., Fuchs, S., 2008. Benefits of local structural protection to mitigate torrent-related hazards, in Risk Analysis VI, edited by C. Brebbia and E. Beriatos, pp. 401-411, WIT, Southampton.

Holub, M., Fuchs, S., 2009. Mitigating mountain hazards in Austria – Legislation, risk transfer, and awareness building. Natural Hazards and Earth System Sciences, 9, 523-537, DOI: https://doi.org/10.5194/nhess-9-523-2009.

Holub, M., Suda, J., S. Fuchs, S., 2012. Mountain hazards: reducing vulnerability by adapted building design, Environmental Earth Sciences, 66(7), 1853-1870. DOI: https://doi.org/10.1007/s12665-011-1410-4.

Hu, K. H., Cui, P., Zhang, J. Q. , 2012. Characteristics of damage to buildings by debris flows on 7 August 2010 in Zhouqu, Western China, Natural Hazards and Earth System Sciences, 12(7), 2209-2217. DOI: 10.5194/nhess-12-2209-2012.

Hungr, O., 2008. Numerical modelling of the dynamics of debris flows and rock avalanches. Geomechanics and Tunnelling, 1, 112-119, DOI: https://doi.org/10.1002/geot.200800010.

Italian Building Code, 2008. Technical recommendations for buildings and commentary (D.M. 14/01/2008 and Circolare 02/02/2009). Rome, Italy (in Italian)

Iverson, R., 2004. Debris flow. In: Goudie, A., editor. Encyclopedia of geomorphology. Routledge, London, 225.

Jakob, M., Hungr, O., 2005. Debris-flow hazards and related phenomena. Chichister: Praxis Publishing, DOI: https://doi.org/10.1007/b138657.

Jakob, M., Stein, D., Ulmi, M., 2012. Vulnerability of buildings to debris flow impact. Natural Hazards, 60, 241-261, DOI: https://doi.org/10.1007/s11069-011-0007-2.

Karagiorgos, K., Thaler, T., Hübl, J., Maris, F., Fuchs, S., 2016. Multi-vulnerability analysis for flash flood risk management. Natural Hazards, 82(1), 63-87. DOI: https://doi.org/10.1007/s11069-016-2296-y.

Karvonen, R.A., H. K. Hepojoki, H. K. Huhta and A. Louhio, 2000. The use of physical models in dam-break flood analysis, Development of Rescue Actions Based on Dam-Break Flood Analysis (RESCDAM). Final report of Helsinki University of Technology, Finnish Environment Institute, Helsinki, Finland.

Keiler, M., Knight, J., Harrison, S., 2010. Climate change and geomorphological hazards in the eastern European Alps. Philosophical Transactions of the Royal Society of London. Series

A: Mathematical, Physical and Engineering Sciences, 368, 2461-2479, DOI: 10.1098/rsta.2010.0047.

Kelman, I., Spence, R., 2003. A limit analysis of unreinforced masonry failing under flood water pressure. Masonry International, 16, 51-61.

Kienholz, H., Krummenacher, B., Kipfer, A., Perret, S., 2004. Aspects of integral risk management in practice – considerations with respect to mountain hazards in Switzerland. Österreichische Wasser- und Abfallwirtschaft, 56, 43-50.

Lo, W.-C., Tsao, T.-C., Hsu, C.-H., 2012. Building vulnerability to debris flows in Taiwan: a preliminary study. Natural Hazards, 64, 2107-2128, DOI: https://doi.org/10.1007/s11069-012-0124-6.

Loucks, D.P., 2015. Perspectives on socio-hydrology: Simulating hydrologic-human interactions. Water Resources Research, 51 (6), 4789-4794. DOI: https://doi.org/10.1002/2015WR017002.

Lourenco, P. B., 1996. Computational Strategies for Masonry Structures, PhD thesis, Delft University of Technology, Delft, The Netherlands.

Martínez-Gomariz, E., Gómez, M., Russo, B. and Djordjević, S., 2016. Stability criteria for flooded vehicles: a state-of-the-art review. Journal of Flood Risk Management. DOI: https://doi.org/10.1111/jfr3.12262.

Mazzorana, B., Comiti, F., Scherer, C., Fuchs, S., 2012. Developing consistent scenarios to assess flood hazards in mountain streams, Journal of Environmental Management, 94(1), 112-124. DOI: https://doi.org/10.1016/j.jenvman.2011.06.030.

Mazzorana, B., Simoni, S., Scherer, C., Gems, B., Fuchs, S., Keiler, M., 2014. A physical approach on flood risk vulnerability of buildings. Hydrology and Earth System Sciences, 18, 3817-3836, DOI: https://doi.org/10.5194/hess-18-3817-2014.

Milanesi, L., Pilotti, M., Ranzi, R., Valerio, G. 2014. Methodologies for hydraulic hazard mapping in alluvial fan areas, in Evolving Water Resources Systems: Understanding, Predicting and Managing Water–Society Interactions, Proceedings of ICWRS2014, Bologna, Italy, 4–6 June 2014, IAHS Publ. Ser., vol. 364, pp. 267–272, Int. Assoc. of Hydrol. Sci., Wallingford, U. K.

Milanesi, L., Pilotti, M., Ranzi, R., 2015. A conceptual model of people's vulnerability to floods, Water Resources Research, 51(1), DOI: https://doi.org/10.1002/2014WR016172.

Milanesi, L., Pilotti, M., Bacchi, B., 2016. Using web-based observations to identify thresholds of a person's stability in a flow, Water Resources Research, 52, DOI: https://doi.org/10.1002/2016WR019182

Milani, G., Lourenço, P.B., Tralli, A. 2006a. Homogenization Approach for the Limit Analysis of Out-of-Plane Loaded Masonry Walls. Journal of Structural Engineering, 132(10), 1650-1663. DOI: https://doi.org/10.1061/(ASCE)0733-9445(2006)132:10(1650)

Milani, G., Lourenço, P.B., Tralli, A. 2006b. Homogenised limit analysis of masonry walls, Part II: Structural examples. Computers & Structures. 84 (3-4), 181-195, DOI: https://doi.org/10.1016/j.compstruc.2005.09.004

Molinari, D., Ballio, F., Handmer, J., Menoni, S., 2014. On the modeling of significance for flood damage assessment. International journal of disaster risk reduction, 10, 381-391, DOI: https://doi.org/10.1016/j.ijdrr.2014.10.009.

Page, A.W., 1981. The biaxial compressive strength of brick masonry. Proceedings of the Institution of Civil Engineers, Part 2, 71, 893–906.

Page, A.W., 1983. The strength of brick masonry under biaxial tension–compression. Int. J. Masonry Constr. 3(1), 26–31.

Papathoma-Köhle, M., Keiler, M., Totschnig, R., Glade, T., 2012. Improvement of vulnerability curves using data from extreme events: debris flow event in South Tyrol. Natural Hazards, 64, 2083-2105, DOI: https://doi.org/10.1007/s11069-012-0105-9.

Papathoma-Köhle, M., Zischg, A., Fuchs, S., Glade, T., Keiler, M. 2015. Loss estimation for landslides in mountain areas – An integrated toolbox for vulnerability assessment and damage documentation. Environmental Modelling and Software, 63, 156-169, DOI: https://doi.org/10.1016/j.envsoft.2014.10.003.

Papathoma-Köhle, M., Gems, B., Sturm, M., Fuchs, S., 2017. Matrices, curves and indicators: a review of approaches to assess physical vulnerability to debris flows. Earth-Science Reviews, 171, 272-288, DOI: https://doi.org/10.1016/j.earscirev.2017.06.007.

Pilotti, M., Maranzoni, A., Tomirotti, M. and Valerio, G., 2011. The 1923 Gleno dam-break: case study and numerical modelling, Journal of Hydraulic Engineering, 137, 480-492, DOI: https://doi.org/10.1061/(ASCE)HY.1943-7900.0000327.

Pilotti, M., Tomirotti, M., Valerio, G. and Milanesi, L., 2013. Discussion of "Experimental investigation of reservoir geometry effect on dam-break flow" by A. Feizi Khankandi, A. Tahershamsi and S. Soares-Frazão. Journal of Hydraulic Research, 51(2), 220-222, DOI: https://doi.org/10.1080/00221686.2013.765165.

Pilotti M., Maranzoni, A., Milanesi, L., Tomirotti, M., and Valerio, G., 2014. Dam-break modeling in alpine valleys, Journal of mountain science, 11(6), 1429-1441, DOI: https://doi.org/10.1007/s11629-014-3042-0.

Pilotti, M., Milanesi, L., Ranzi, R. 2016. People and buildings vulnerability to floods in mountain areas. In: Koboltschnig, G., editor. Internationales Symposion Interpraevent. Internationale Forschungsgesellschaft Interpraevent, Lucerne, 791-798.

Röthlisberger, V., Zischg, A., Keiler, M., 2017. Identifying spatial clusters of flood exposure to support decision making in risk management. Science of the Total Environment, 598, 593-603, DOI: https://doi.org/10.1016/j.scitotenv.2017.03.216.

Sangrey, D.A., Murphy, P.J., Nieber, J.L., 1975. Evaluating the impact of structurally interrupted flood plain flows. Cornell University. Prepared for: Office of Water Research and Technology. Distributed by: NTIS. PB-247 552.

Santi, P., Hewitt, K., VanDine, D., Barillas Cruz, E., 2011. Debris-flow impact, vulnerability, and response. Natural Hazards, 56, 371-402, DOI: https://doi.org/10.1007/s11069-010-9576-8.

Serre, D., Lhomme, S., Heilemann, K., Hafskjold, L.S., Tagg, A., Walliman, N., Diab, Y., 2011. Assessing vulnerability to floods of the built environment - integrating urban networks and buildings. First International Symposium on Uncertainty Modeling and Analysis and Management (ICVRAM 2011); and Fifth International Symposium on Uncertainty Modeling and Anaylsis (ISUMA), Hyattsville, Maryland, United States.

Soares Frazão, S., and Zech, Y., 2007. Experimental study of dam-break flow against an isolated obstacle. Journal of Hydraulic Research, 45 (Extra Issue), 27–36, DOI: https://doi.org/10.1080/00221686.2007.9521830.

Sturm, M., Gems, B., Keller, F., Mazzorana, B., Fuchs, S., Papathoma-Köhle, M. and Aufleger, M., 2018: Experimental analyses of impact forces on buildings exposed to fluvial hazards. Journal of Hydrology, (in press), DOI:https://doi.org/10.1016/j.jhydrol.2018.07.070.

Thouret, J.-C., Ettinger S., Guitton, M., Santoni, O., Magill, C., Martelli, K., Zuccaro, G., Revilla, V., Charca, J. A., Arguedas, A., 2014. Assessing physical vulnerability in large cities exposed to flash floods and debris flows: the case of Arequipa (Peru), Natural Hazards, 73(3), 1771-1815. DOI: https://doi.org/10.1007/s11069-014-1172-x.

Totschnig, R., Sedlacek, W., Fuchs, S., 2011. A quantitative vulnerability function for fluvial sediment transport. Natural Hazards, 58, 681-703, DOI: https://doi.org/10.1007/s11069-010-9623-5.

Totschnig, R., Fuchs, S., 2013. Mountain torrents: quantifying vulnerability and assessing uncertainties. Engineering Geology, 155, 31-44, DOI: https://doi.org/10.1016/j.enggeo.2012.12.019.

Xia. J., Falconer, R.A., Wang, Y., Xiao X., 2014, New criterion for the stability of a human body in floodwaters, Journal of Hydraulic Research, 52(1), 93-104, DOI: 10.1080/00221686.2013.875073

Yalin, S., 1977. Mechanics of sediment transport. Pergamon Press.

Zanchetta, G., Sulpizio,, R., Pareschi, M., Leoni, F., Santacroce, R., 2004. Characteristics of May 5-6, 1998 volcaniclastic debris flows in the Sarno area (Campania, southern Italy): relationships to structural damage and hazard zonation, Journal of Volcanology and Geothermal Research, 133(1-4), 377-393. DOI: https://doi.org/10.1016/S0377-0273(03)00409-8.

Zanuttigh, B., Lamberti, A., 2006. Experimental analysis of the impact of dry avalanches on structures and implication for debris flows. Journal of Hydraulic Research, 44(4), 522-534, DOI: https://doi.org/10.1080/00221686.2006.952170

Zimmermann, M., Keiler, M., 2015. International frameworks for disaster risk reduction: useful guidance for sustainable mountain development? Mountain Research and Development, 35, 195-202, DOI: https://doi.org/ 10.1659/MRD-JOURNAL-D-15-00006.1.

Tab. 1 – Values of α as a function of shape factor (X_1) and vertical load (X_3).

Case geometry and load		P3 (3-edges support)	P4 (4-edges support)
X_3=0	X_1=1	33°	30°
	X_1=2	36°	37°
X_3=1	X_1=1	33°	30°
	X_1=2	30°	36°
X_3=2	X_1=1	33°	29°
	X_1=2	23°	34°

Tab. 2 – Results of the sensitivity analysis expressed as variation of the dimensionless critical flood depth (X_4) for the reference wall P2.

Case geometry and load		0.5 E	2 E	0.5 f_c	2 f_c	0.5 f_t	2 f_t
X_3=0	X_2=0.1	+0.39%	-0.34%	-0.17%	+0.67%	-4.83%	+8.27%
X_3=0	X_2=0.2	+0.21%	-0.62%	-0.36%	+0.41%	-6.25%	+9.13%
X_3=2	X_2=0.1	-1.29%	+0.85%	-0.56%	+0.26%	-7.29%	+5.15%
X_3=2	X_2=0.2	-2.06%	+0.41%	-0.44%	-0.19%	-6.19%	+8.25%

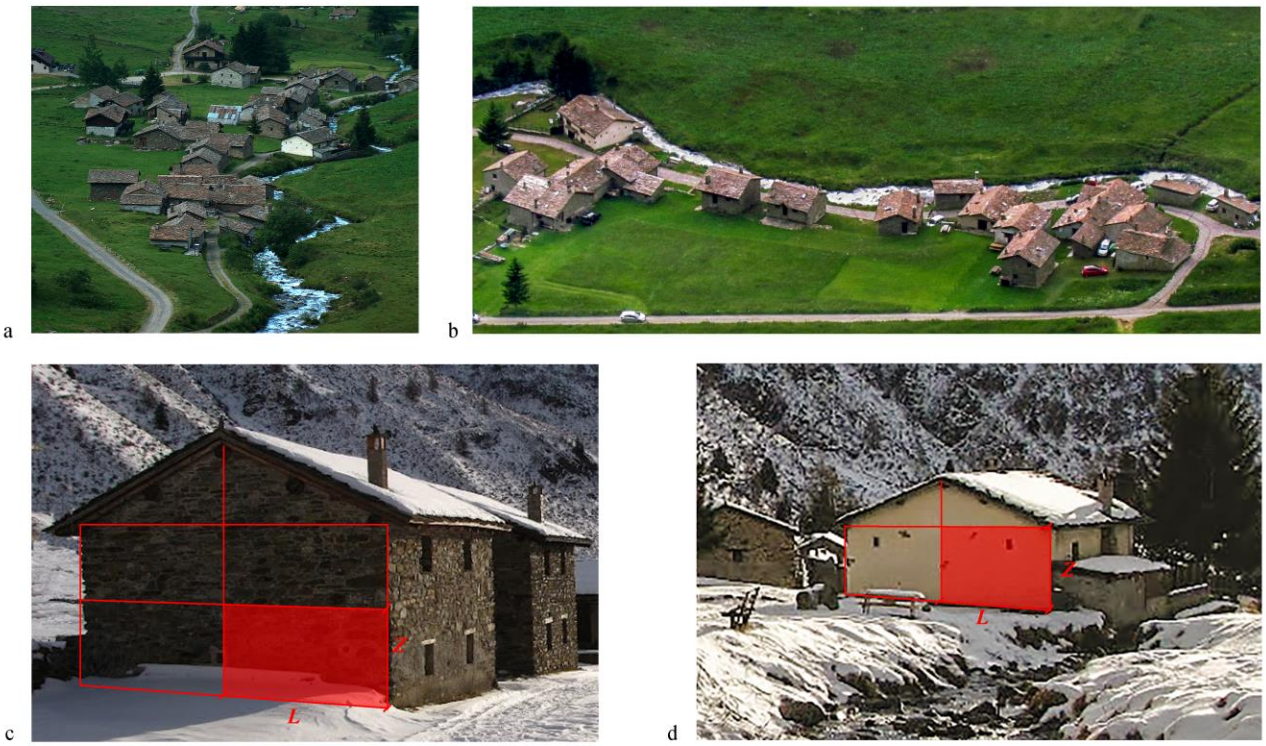

Fig. 1 – A traditional alpine village with a large stock of exposed masonry buildings in the Province of Brescia (Northern Italy) (a, b) and two examples of masonry buildings with indication of the most exposed walls (c, d).

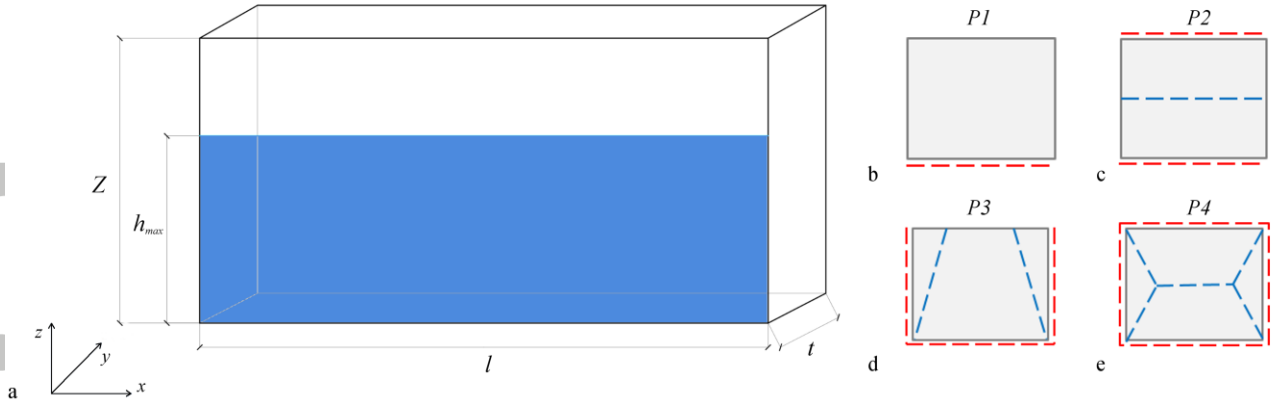

Fig. 2 – a) Front view of the reference wall impacted by the flow; b-e) considered constraints configurations of the reference walls.

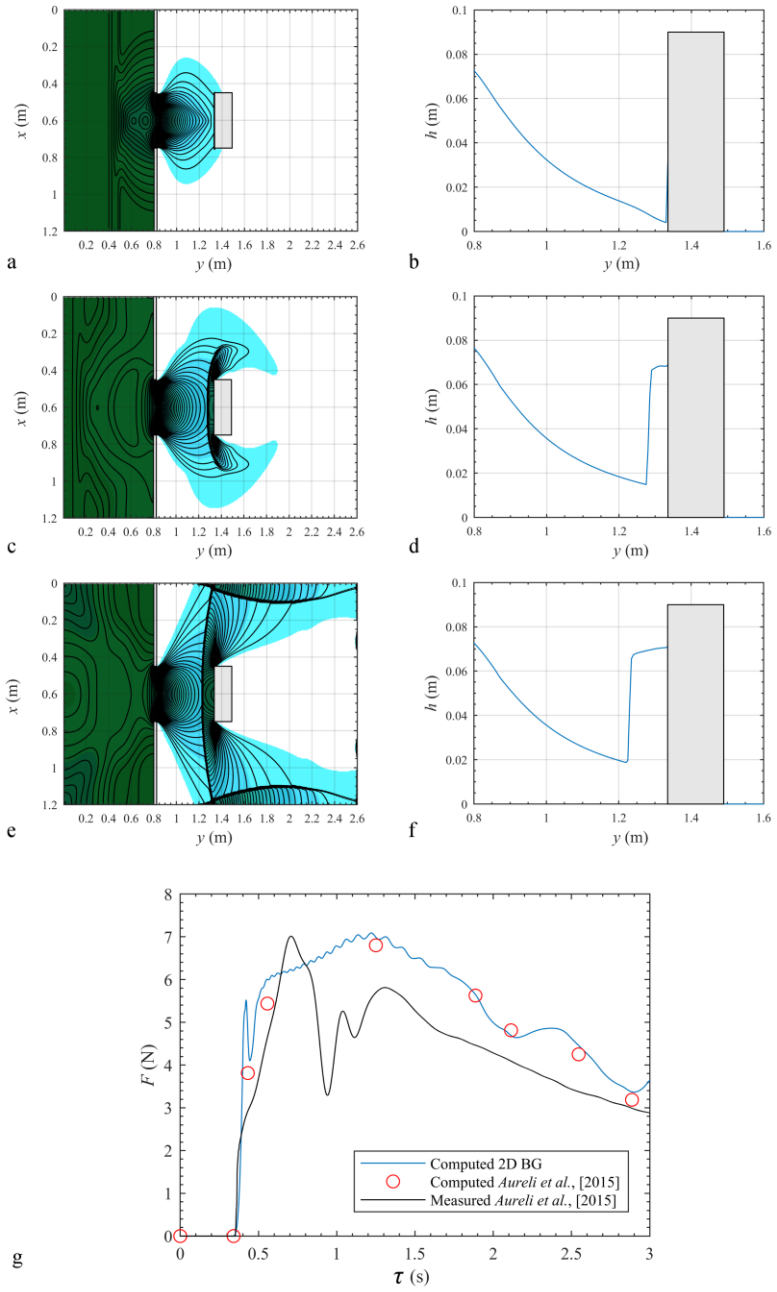

Fig. 3 – Water depth contour maps (left) and longitudinal water surface profile (y=0.6 m; right) at τ = 0.38 s (a, b), τ = 0.71 s (c, d), and τ = 1.44 s (e, f) computed with the 2D BG solver. (g) Force on the obstacle as a function of time. The solid black line is the average force measured by *Aureli et al.* [2015] and the red dots make reference to the results of their 2D numerical model. The blue solid line is computed with the 2D BG solver.

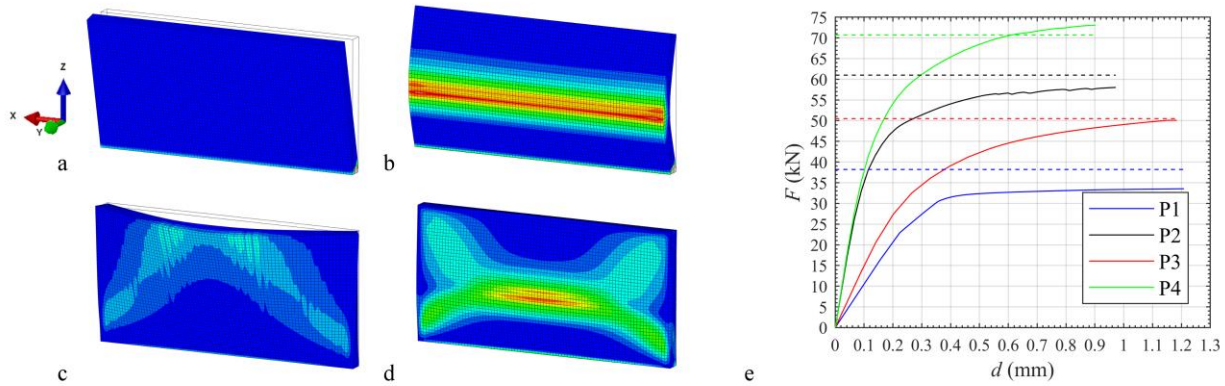

Fig. 4 – Snapshot of the wall deflection as computed by FEM analysis at failure (deflection amplified for clarity of representation, maximum principal plastic strains increasing from blue to red shading). The results qualitatively represent the location of tensile plastic strains for walls P1 (a), P2 (b), P3 (c), and P4 (d). e) Results of the FEM analysis in terms of flood load F (kN) versus maximum out-of-plane deflection d (mm); the dashed lines represent the maximum admissible load predicted by the simplified model presented in Section 2.4.

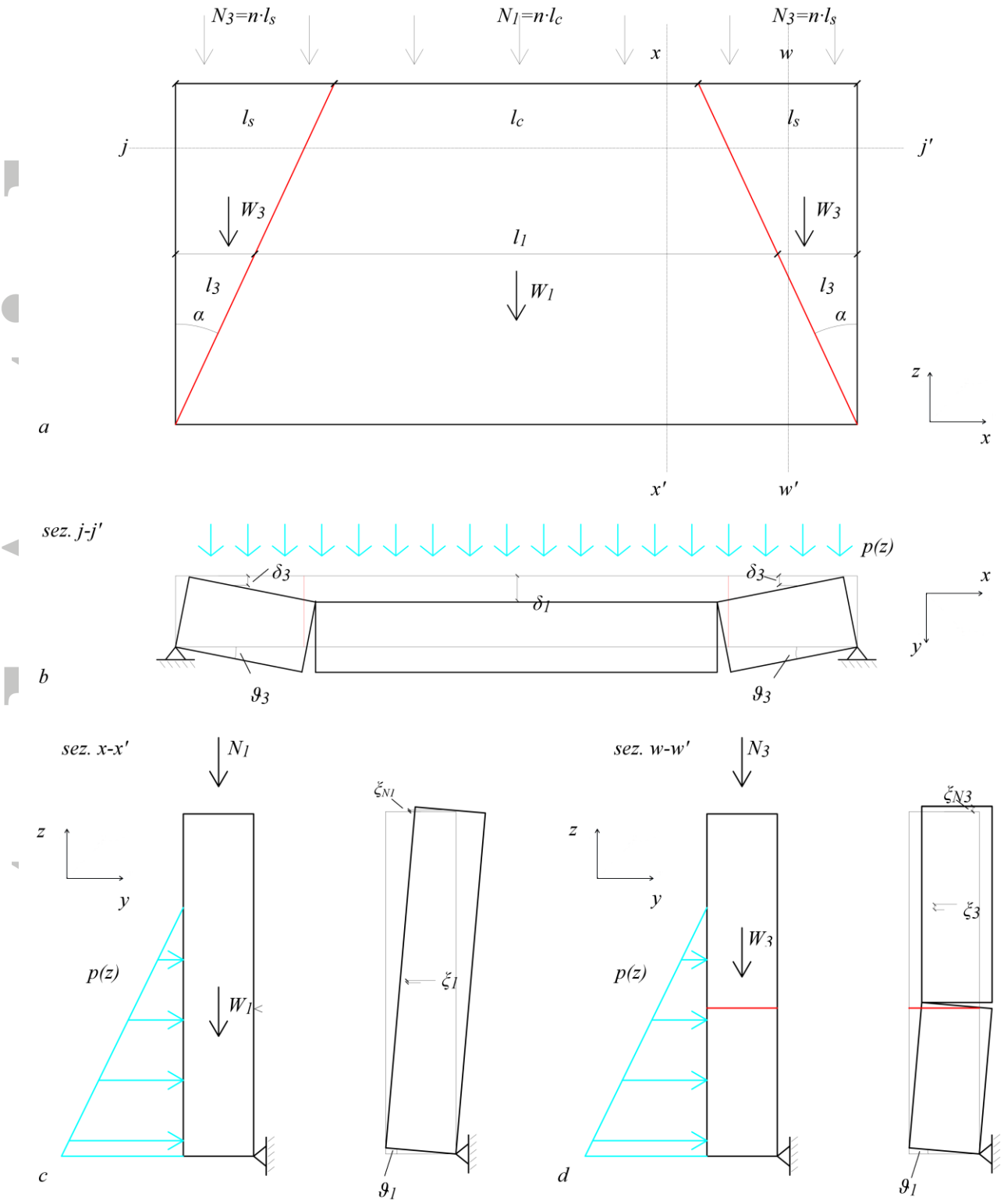

Fig. 5 – Reference wall P3 (3-edges support) collapse mechanism. Front view (a), plan cross section (b) and vertical cross sections (c, d).

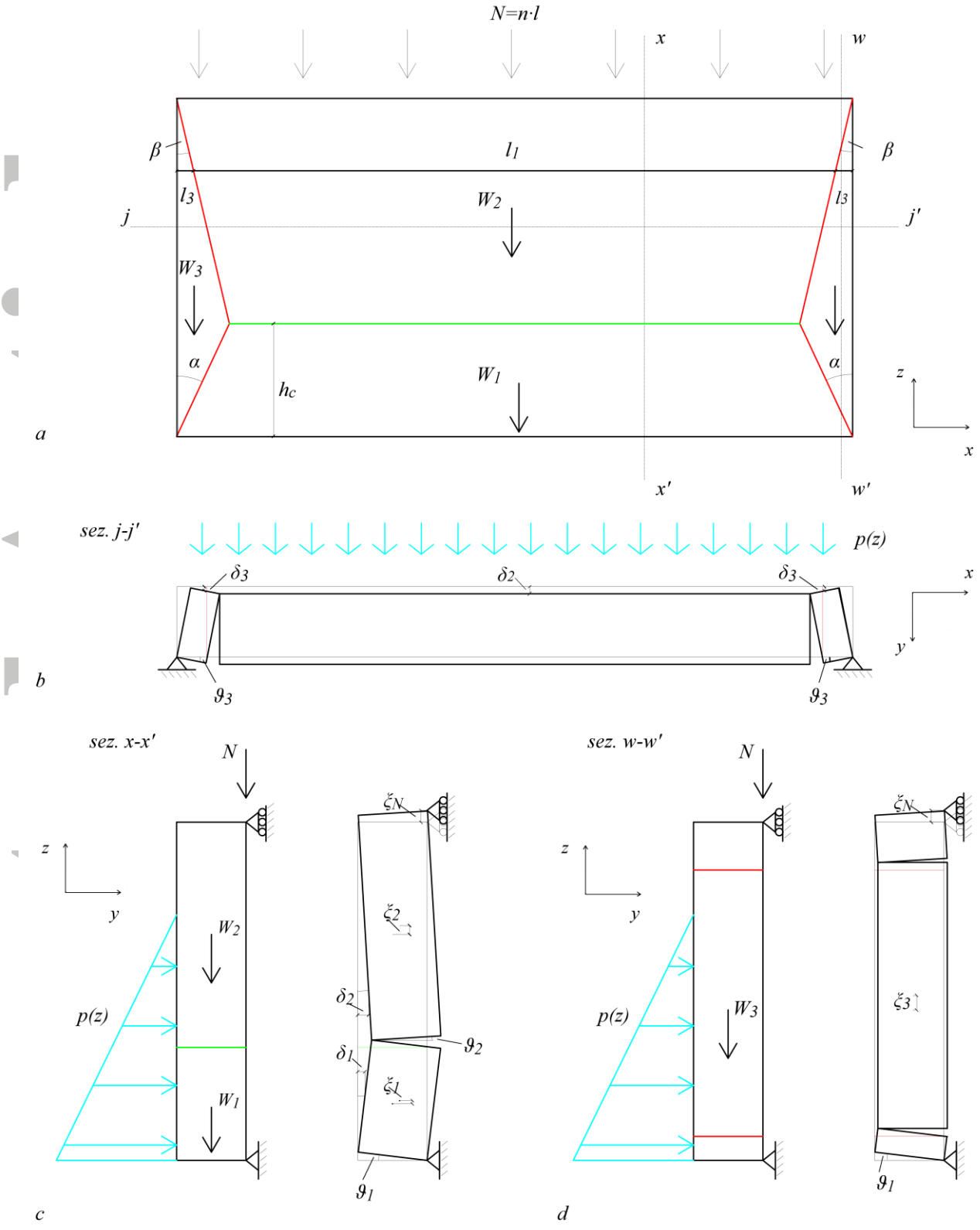

Fig. 6 - Reference wall P4 (4-edges support) collapse mechanism. Front view (a), plan cross section (b) and vertical cross sections (c, d).

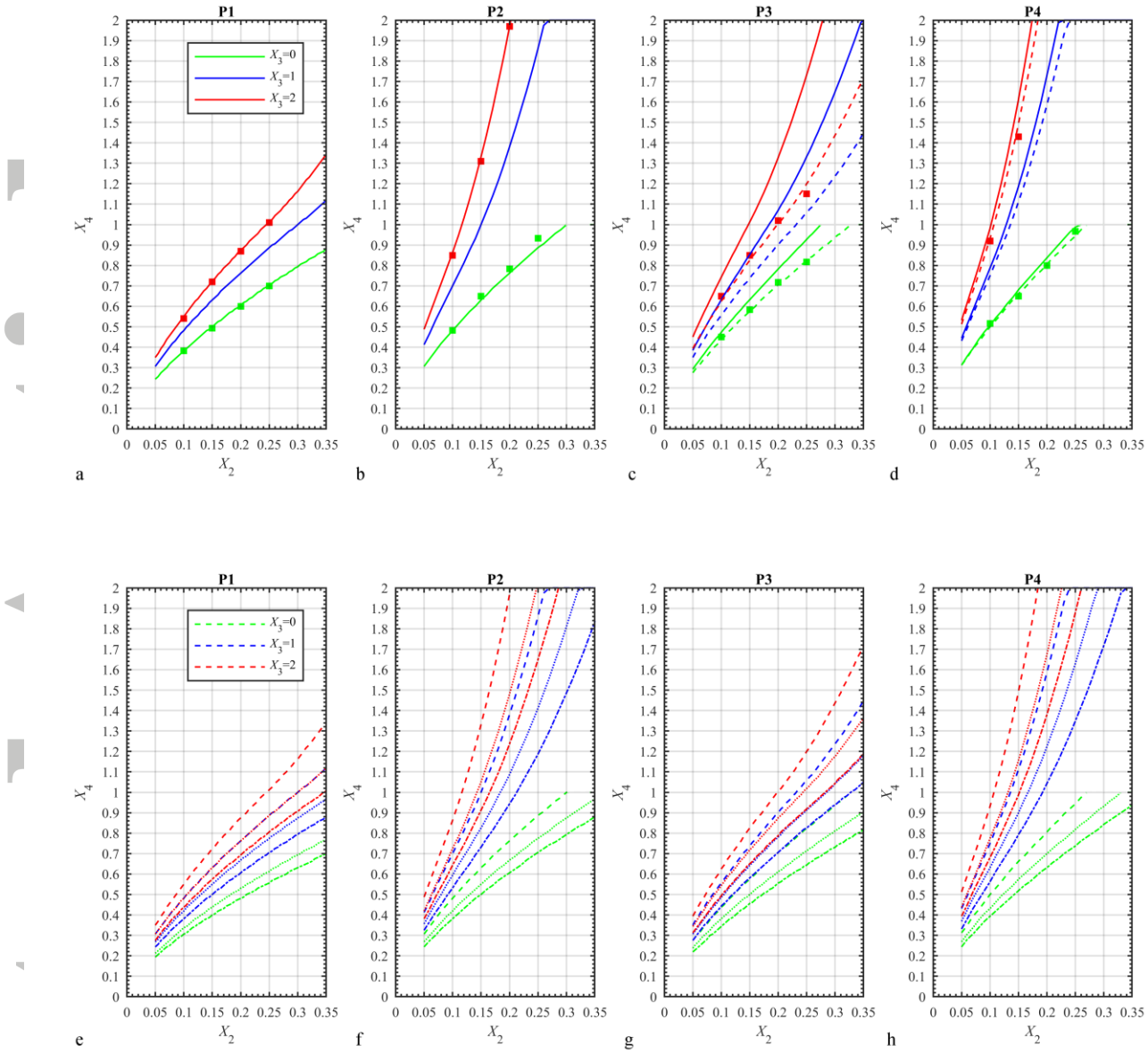

Fig. 7 - Vulnerability thresholds for the reference walls P1 (a), P2 (b), P3 (c), and P4 (d) as a function of the slenderness of the wall (X_2) in case of impact due to a water flow (i.e. X_5=0.56). The solid line plots are computed for wall aspect ratio (X_1) equal to 1 and the hatched lines for X_1=2. The solid dots represent the results of the FEM models referred to the case X_1=2, accordingly they should match the dashed lines. Vulnerability thresholds associated to increased fluid density for the cases P1 (e), P2 (f), P3 (g – only for X_1=2), and P4 (h – only for X_1=2). The dashed lines are related to X_5=0.56, the dotted lines to X_5=0.83 and the stretch-point lines to X_5=1.11.

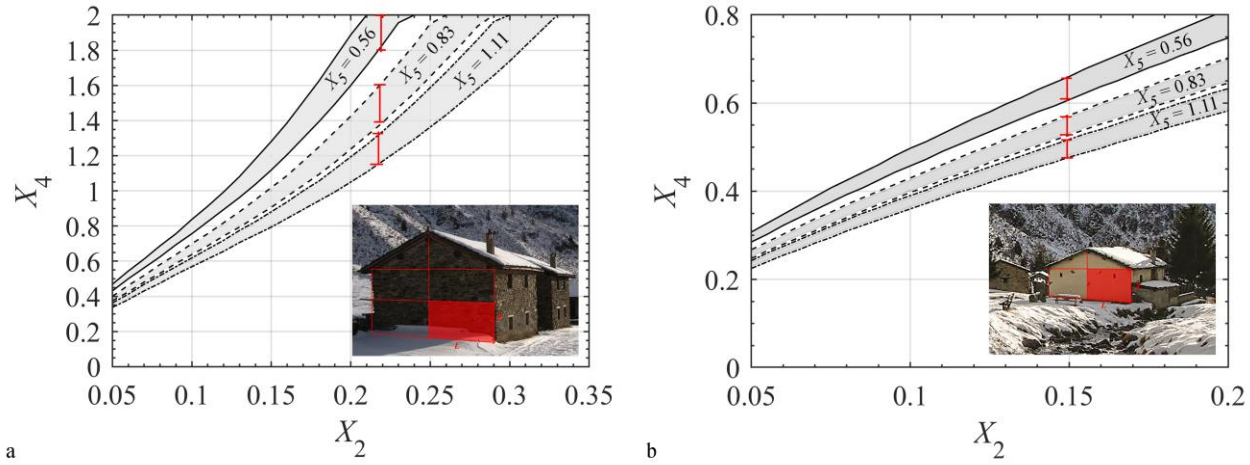

Fig. 8 - Examples of traditional masonry buildings from the village shown in Fig. 1. The red shadings show the elementary wall units modelled with the simplified model. The stability bands are computed considering the variability of the geometric parameters of the buildings, and some different relative density values (X5).

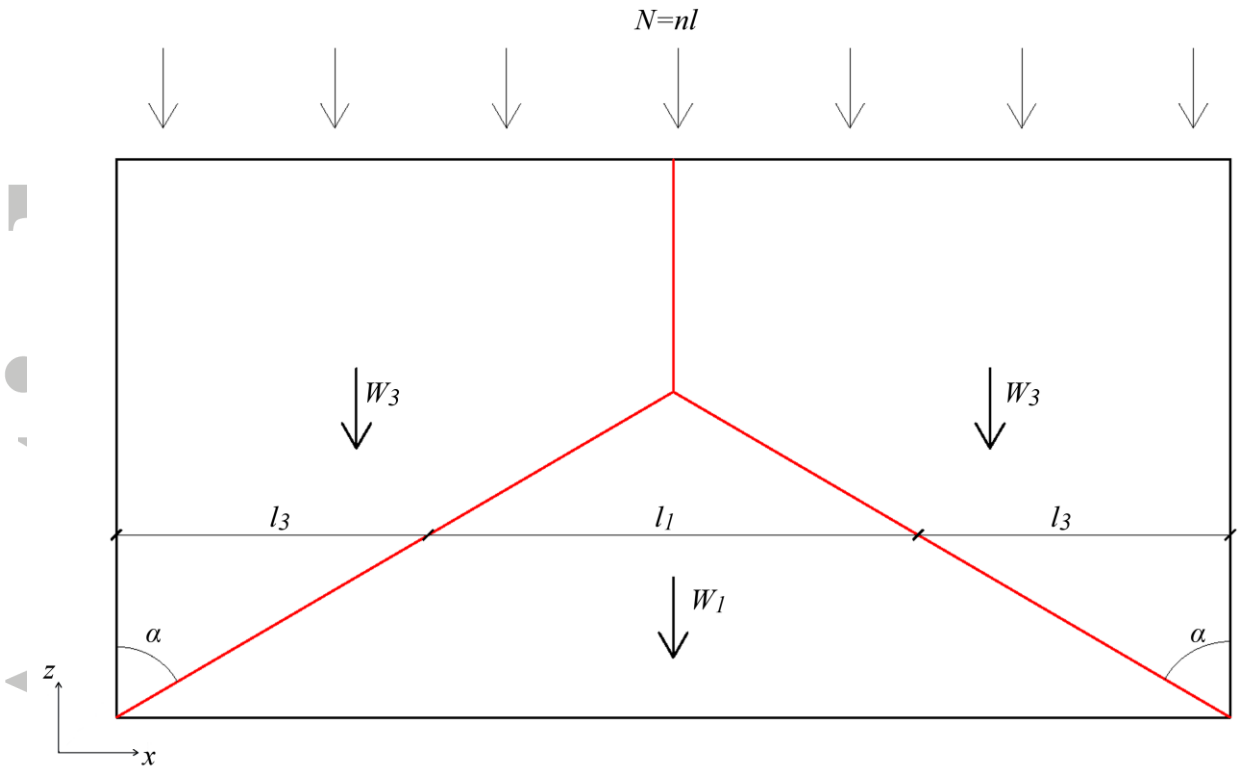

Fig. A1 – Reference wall P3 (3-edges support) collapse mechanism when fracture lines intersect inside the wall panel.